Measurement Science and Technology

100 year anniversary
Measurement Science and Technology

PAPER • OPEN ACCESS

A comprehensive study on temple clamping force for eyeglasses design: from measuring to modelling

To cite this article: Jie Zhang *et al* 2024 *Meas. Sci. Technol.* **35** 105903

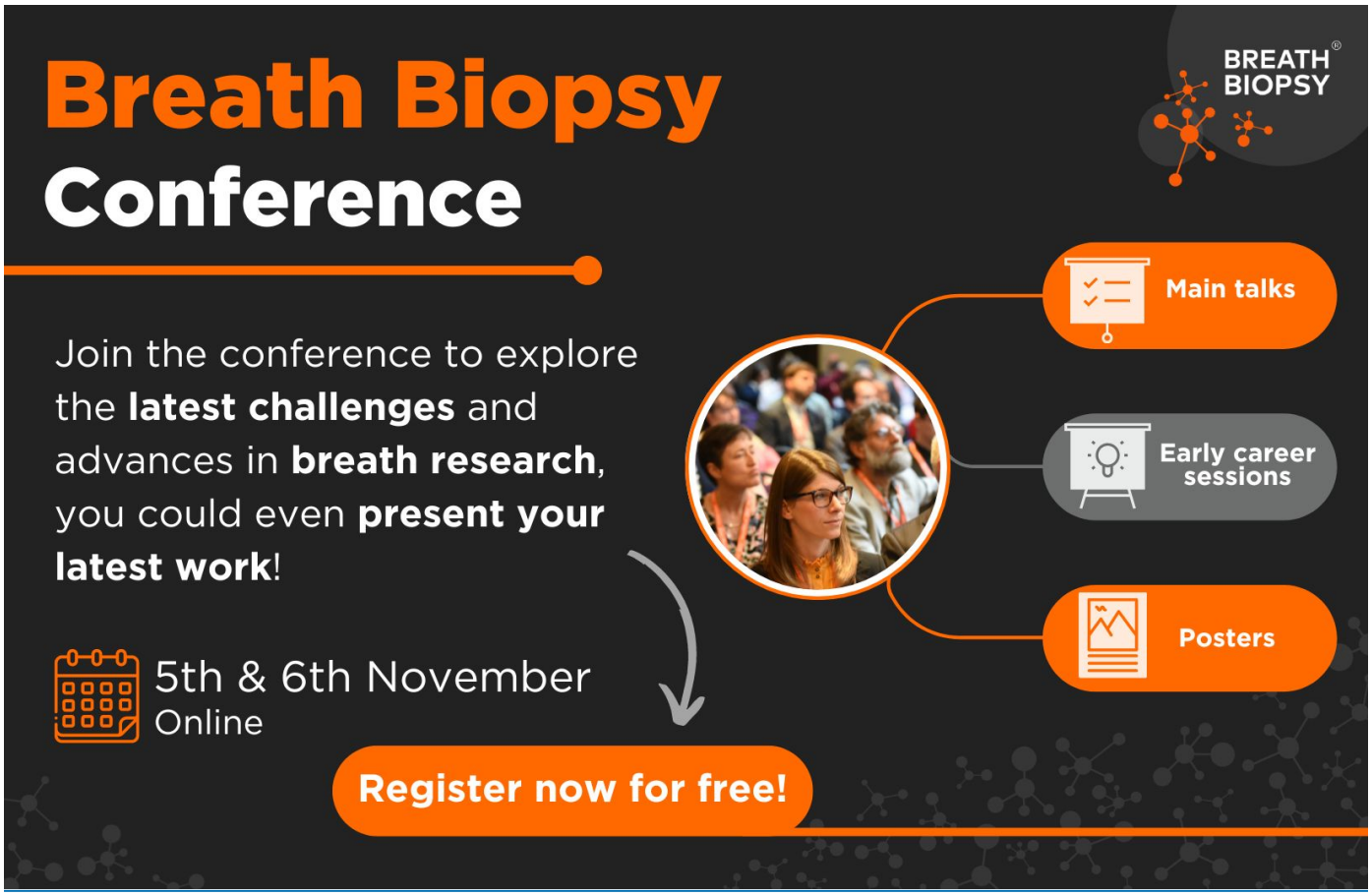

OPEN ACCESS
IOP Publishing
Measurement Science and Technology
Meas. Sci. Technol. **35** (2024) 105903 (12pp)
https://doi.org/10.1088/1361-6501/ad5a2d

A comprehensive study on temple clamping force for eyeglasses design: from measuring to modelling

Jie Zhang[1,3], **Junjian Chen**[2,3] and **Yan Luximon**[2,3,*]

[1] Faculty of Applied Sciences, Macao Polytechnic University, Macao Special Administrative Region, People's Republic of China
[2] School of Design, The Hong Kong Polytechnic University, Hong Kong Special Administrative Region of China, People's Republic of China
[3] Laboratory for Artificial Intelligence in Design, Hong Kong Science Park, Hong Kong Special Administrative Region of China, People's Republic of China

E-mail: yan.luximon@polyu.edu.hk

Received 12 March 2024, revised 3 June 2024
Accepted for publication 20 June 2024
Published 9 July 2024

Abstract

A key factor in determining the comfort level of eyeglasses is the clamping force at the temple. However, how to accurately measure and estimate the clamping force remains under-explored. Hence, to address this gap, we proposed a novel temple clamping force measurement method with a digital tension meter and developed a mathematical model to calculate the clamping force of the temples based on eyeglasses parameters (including length, one-side displacement, and flexural rigidity of the temples). To validate our method, we collected the simulated and physical datasets of different eyeglasses and conducted a multiple regression analysis to calculate the model parameters. The experimental results demonstrated the accuracy and reliability of the proposed method. This model can guide us in customizing the parameters of the eyeglasses to produce comfortable clamping forces for the users. Our codes and data will be publicly available at: https://github.com/Easy-Shu/Eyeglasses_Force_Modelling.

Keywords: measuring temple clamping force, modeling temple clamping force, eyeglasses design, finite element analysis

1. Introduction

Eyeglasses, consisting of a frame and lenses, are widely used devices worn on the face to correct refractive errors and improve visual acuity. They also serve other purposes, e.g. increasing facial attractiveness, and transferring information. As per the World Health Organization's report [1], around 2.2 billion individuals globally have some degree of vision impairment, out of which at least 1 billion could have avoided or addressed their vision impairment. This indicates that there is a high demand for eyeglasses to improve their vision. Augmented reality (AR) glasses, in particular, have revolutionized the way people interact with digital content and perform various tasks. A recent report by Grand View Research [2] indicates that the global market size for augmented reality was valued at USD 25.33 billion in 2021 and is projected to grow at a compound annual growth rate of 40.9% from 2022 to 2030. This suggests that an increasing number of people will use AR glasses. Regardless of personalization and mass customization of eyeglasses, ensuring a high level of perceived comfort remains a critical objective.

The temples are an essential component of most glasses, including those for myopia, hyperopia, astigmatism, sunglasses, and AR glasses. The clamping force exerted by

[3] Contributed equally to this paper.
[*] Author to whom any correspondence should be addressed.

the temples is a critical factor in determining comfort levels for the wearer [3, 4]. Too much clamping force can cause pain in the ear attachment area, while too little force may not provide enough friction to prevent the eyeglasses from sliding. Therefore, it is crucial to determine the optimal clamping force to enhance the comfort of glasses for the wearers. To accurately measure and estimate the clamping force of the temples, it is essential to establish a foundation for comfortable clamping force levels. The primary challenge in this research was accurately measuring and modelling the clamping force of eyeglass temples. Developing reliable measurement and modelling methods is difficult, as the force can be influenced by various factors, such as eyeglass frame design and individual head geometry. Researchers had to account for the shape and materials of the frame, as well as the unique contours of each wearer's face and ears, which can significantly impact the pressure exerted by the temples. Additionally, personal sensitivity to this pressure can vary across individuals, making it challenging to establish universal standards for comfort.

Measuring clamping force In previous research, different types of strain gauges have been utilized to measure the clamping force of eyeglass temples. For instance, Du *et al* [5] measured the temple clamping force of the eyeglasses prototype by using a FlexiForce®A201 strain gauge on its head contact regions. In contrast, Kouchi *et al* [6] and Mashima *et al* [7] used a similar technique by applying a Kyowa strain gauge to the medial (lateral) side of the temple to measure the clamping force. However, these strain gauges typically have a sensing area with a diameter larger than the temple height (which ranges from 1.0 mm to 6.0 mm), and their lowest measurable force is sometimes higher than the clamping forces (which range from 0.0 N to 1.0 N). As Saadeh *et al* [8] have pointed out, this could potentially lead to inaccurate and unreliable measurements of the temple clamping force on the ear regions. Therefore, to solve these limitations of using strain gauges to measure the clamping force of the temple, it is essential to explore alternative methods that may provide more accurate and reliable results.

Modelling clamping force Accurately estimating temple clamping force for different wearers and validating measuring results is a significant issue for glasses ergonomic design and virtual try-on. One promising approach is to model the clamping force, which can provide valuable insights into product personalization and sizing system establishment. For instance, by combining a quantified comfort perception model with the clamping force model, it becomes possible to predict the perceived comfort scores for individual users based on their clamping forces. Despite the potential benefits, the specific quantified relationships between clamping force, materials, displacement, and temple length remain largely unknown. However, it requires further research and exploration to identify their specific quantified relationships. A comprehensive understanding of these relationships would enable glasses manufacturers to optimize their products that provide the higher level of comfort and satisfaction for their customers. Moreover, it would provide valuable insights into the development of virtual try-on applications that can accurately simulate the user's experience with the product.

In this study, instead of using strain gauges, we presented a novel device based on a digital tension meter to measure the clamping force at the temples indirectly. We also developed a mathematical model to calculate the clamping force of the temples based on key eyeglasses parameters, including length, displacement, and flexural rigidity of the temples. To construct the mathematical model, we adopted Bernoulli-Euler beam theory [9] as the theoretical foundation. This allowed us to derive an approximate model for calculating the clamping force. Furthermore, we utilized finite element analysis (FEA) to simulate the behavior of digital eyeglasses. This FEA approach generated a range of simulated data that captured various temple displacements caused by different clamping forces and temple lengths. We then used this simulated data to validate the mathematical model through multiple regression analysis [10, 11]. Finally, we used the developed measurement device to obtain physical data on the clamping forces of actual eyeglasses. We were then able to further validate the mathematical model by comparing the predictions from the model against these physical measurements. While our previous conference paper [12] focused solely on the clamping force measurement, this paper extends that work to a more comprehensive study of temple clamping force and presents a significant contribution in measuring, modeling, and perceiving the temple clamping force. This provides a reliable and efficient solution for manufacturers to optimize the design and production of eyewear products, ultimately improving the quality and comfort of the end-user experience.

2. Method

2.1. Measuring clamping force

In this study, we adopted an offline clamping force measurement technique by measuring the static and wearing expanded distances of the ear attachment points (EAPs) at the temple (see figure 1) with the same displacement instead of measuring the online clamping force. A device was designed and manufactured to measure the clamping force using a digital tension meter, as shown in figure 2). During the experiment, the tension meter was moved from its initial position (with a tensile force: 0 N) to a new position (with a new tensile force) using a rotating screw while the eyeglasses frame was held in place, and the movement distance is equal to the one-side temple's displacement d. At this new position, the measured tensile force corresponds to the clamping force experienced by the participant when wearing the eyeglasses frame, as the reaction and action forces are reciprocal at the temples.

For each participant, the static W_{st} and wearing W_{wt} expanded distances of the EAPs on the temple (see figure 1) can be measured using a digital vernier and spreading caliper,

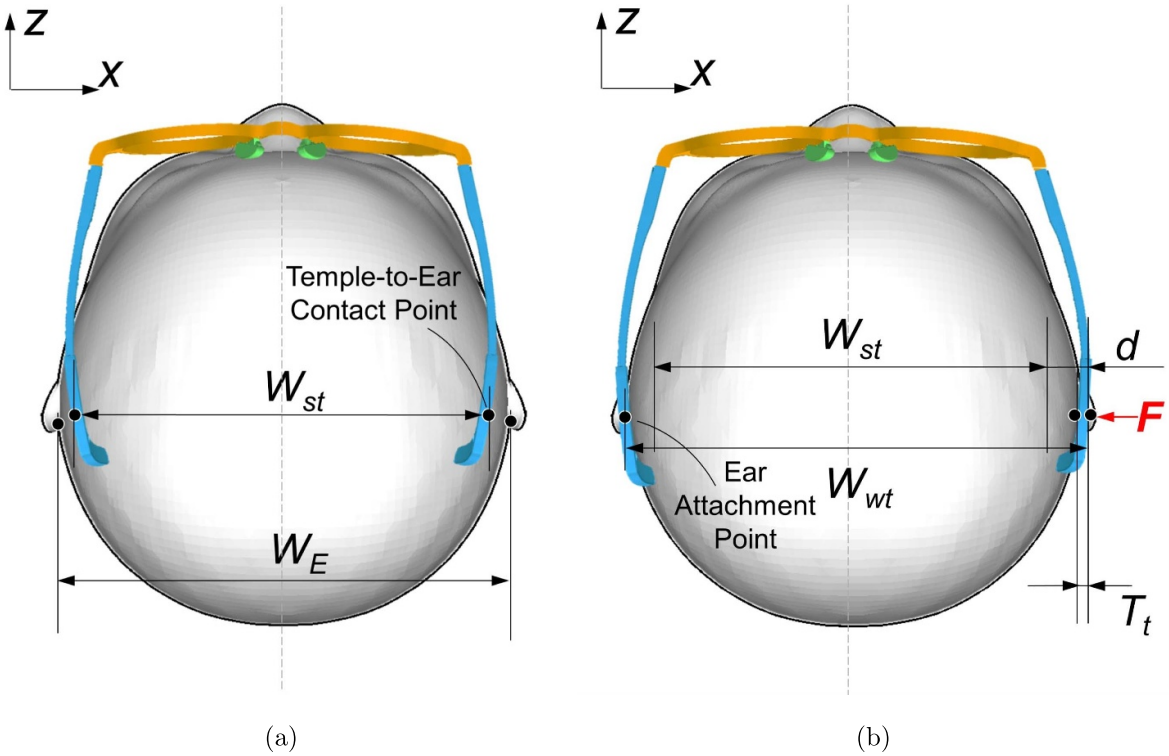

Figure 1. Eyeglasses with a symmetric human head under (a) static condition and (b) wearing condition. F: the clamping force of one-side temple. W_{st} (W_{wt}): the expansion lateral distance of two ear attachment points (EAPs) at the temples under static (wearing) condition. W_E: the lateral distance between left and right EAPs on the head surface (head width). d: displacement of EAPs. T_t: the thickness of the temple around EAPs.

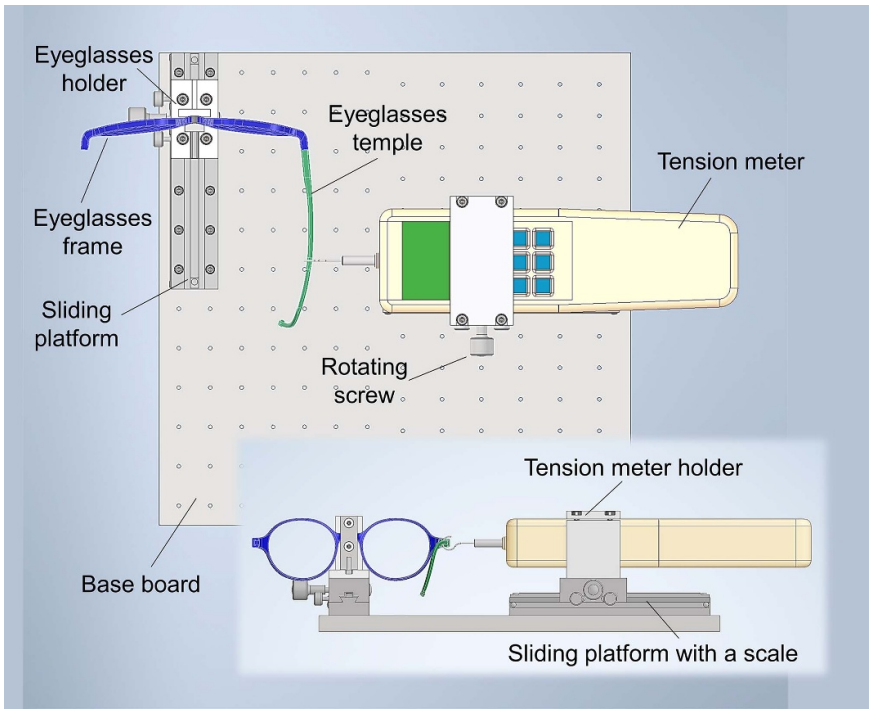

Figure 2. Temple clamping force measurement using a digital tension meter (Model: SH-2, Shanghai Siwei Instrument Manufacturing Co., Ltd Shanghai) with a resolution of 0.001 N and a range of 0 N to 2 N. The measurement points of the temple for the tension meter is corresponding to the ear attachment points (EAPs) in figure 1.

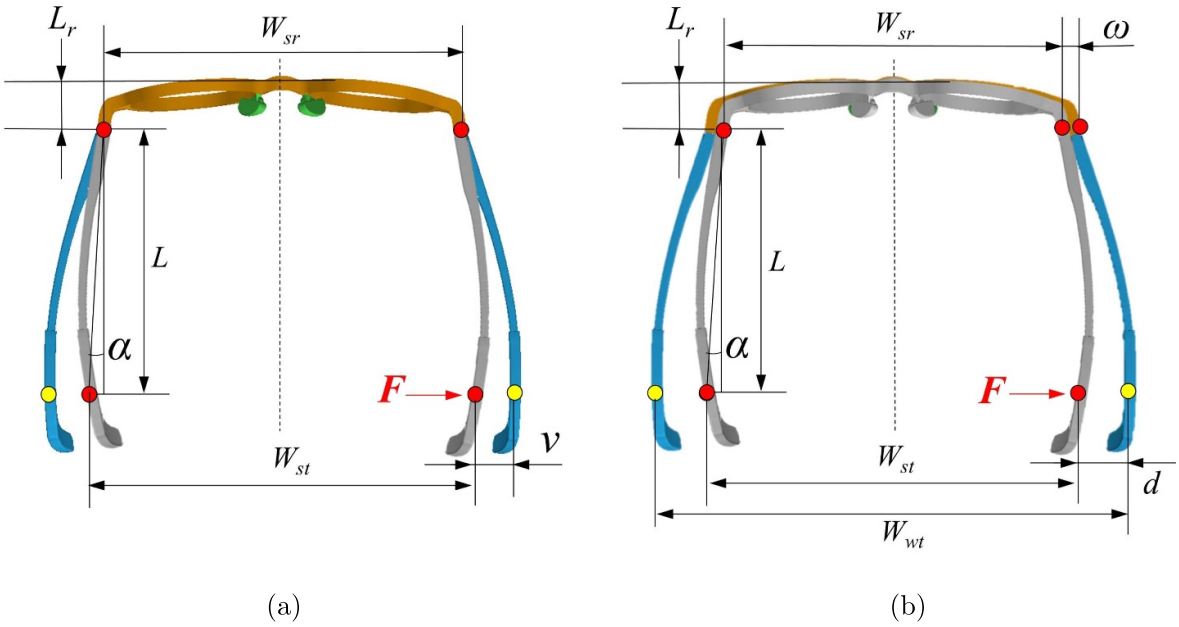

Figure 3. Illustration of eyeglasses frame changes. (a) Temple displacement ν of the ear attaching point (EAP) when the rim is fixed, (b) rim displacement ω and superposed displacement d of EAP. Yellow component: rim; blue/gray component: temples under wearing/static condition; and green component: nose pads. L: the temple length; α: the temple expansion angle under static condition; L_r: the rim length; W_{sr}: the rim width under static condition; W_{st} (W_{wt}): the expansion distance of the ear attachment points on the temple under static (wearing) condition.

respectively. In essence, $W_{wt} = W_E + T_t$, where T_t is the thickness of the temple. As the eyeglasses are symmetric, the displacement d of the EAP for one temple can be obtained from $d = (W_{we} - W_{se})/2$. Thus, the displacement d can be calculated as,

$$d = (W_{wt} - W_{st})/2 = (W_E + T_t - W_{st})/2. \tag{1}$$

When the eyeglasses with the known T_t is given, W_{wt} can also be computed using W_E that can also be measured using a spreading caliper or calculated using predefined left/right EAPs on the parameterized head mesh [13, 14].

2.2. Modeling clamping force

When a spectacle frame is worn on a face, the deformation of the middle plane (bridge) is nearly in-deformed and only the temple and frame are significantly and slightly displaced laterally and symmetrically under normal conditions, respectively. Hence, the lateral displacement of temple-and-EAP for spectacle frames consists of two parts (see figure 3(a)): (1) temple displacement ω, and (2) rim displacement ν.

2.2.1. Temple displacement. The temple can be considered as a cantilever beam with the point load F at the EAP ($x = L$). Hence, the wearing clamping force of temple-and-EAP for spectacle frames can be further analyzed by using a cantilever beam model. The moment $M(x)$ at any point between the fixed end and the attachment point is,

$$M(x) = F \cdot (L - x). \tag{2}$$

Although the temple does not fit the Bernoulli–Euler assumptions well, the deformation might still be predicted by the Bernoulli–Euler Beam theory [9]. The Bernoulli–Euler Beam equation for a cross-section of a beam under the Bernoulli-Euler assumptions is,

$$\frac{d^2\nu}{dx^2} = \frac{M}{E \cdot I}, \tag{3}$$

where v is the deflection, M is the internal moment, E is Young's module, and I is the area moment of inertia of the cross-section. When the cross-section varies along the beam (temple), the area moment of inertia will become a function $I(x)$. At different locations, the internal moment is usually different, so that the M will be $M(x)$. The Bernoulli–Euler equation becomes:

$$\frac{d^2\nu}{dx^2} = \frac{M(x)}{E \cdot I(x)}. \tag{4}$$

Theoretically, in a mechanical model of cantilever beam, the deflection ν (see figure 3(a)) of the force exerting point can be described as,

$$\nu = \int_0^L \left(\int_0^L \frac{M(x)}{E \cdot I(x)} dx \right) dx, \tag{5}$$

where E is elastic module determined by the material itself (e.g. E of steel is 207 GPa), $M(x) = F \cdot (L - x)$, L the distance between the force exerting point and the root, and $I(x)$ is the area moment of inertia. When $L = n \cdot \Delta x$, n is the number of sections and Δx is the distance between two sequential sections, the deflection v at the attaching point ($x = L$) can be further described as follows,

$$
\begin{aligned}
\nu \quad &\cong \sum_{0}^{L}\left(\sum_{0}^{L}\frac{M(x)}{E\cdot I(x)}\Delta x\right)\Delta x \\
&= \left(\left(\frac{n\cdot M(0)}{E\cdot I(0)}\right)\Delta x+\left(\frac{(n-1)\cdot M(\Delta x)}{E\cdot I(\Delta x)}\right)\Delta x+\ldots+\left(\frac{2\cdot M((n-2)\cdot\Delta x)}{E\cdot I((n-2)\cdot\Delta x)}\right)\Delta x+\left(\frac{M((n-1)\cdot\Delta x)}{E\cdot I((n-1)\cdot\Delta x)}\right)\Delta x\right)\Delta x \\
&= \left(\frac{n\cdot F\cdot(L-0)}{E\cdot I(0)}+\frac{(n-1)\cdot F\cdot(L-\Delta x)}{E\cdot I(\Delta x)}+\ldots+\frac{2\cdot F\cdot(L-(n-1)\cdot\Delta x)}{E\cdot I((n-2)\cdot\Delta x)}+\frac{F\cdot(L-(n-1)\cdot\Delta x)}{E\cdot I((n-1)\cdot\Delta x)}\right)(\Delta x)^2 \\
&= F\cdot\left(\frac{n\cdot(L-0)}{E\cdot I(0)}+\frac{(n-1)\cdot(L-1\cdot\Delta x)}{E\cdot I(\Delta x)}+\ldots+\frac{2\cdot(L-(n-1)\cdot\Delta x)}{E\cdot I((n-2)\cdot\Delta x)}+\frac{1\cdot(L-(n-1)\cdot\Delta x)}{E\cdot I((n-1)\cdot\Delta x)}\right)(\Delta x)^2 \\
&= F\cdot\left(\sum_{i=0}^{n-1}\frac{(n-i)\cdot(L-i\cdot\Delta x)}{E\cdot I(i\cdot\Delta x)}\right)(\Delta x)^2. \qquad (6)
\end{aligned}
$$

Let $K_t(L,n)=(\sum_{i=0}^{n-1}\frac{(n-i)\cdot(L-i\cdot\Delta x)}{E\cdot I(i\cdot\Delta x)})(\Delta x)^2$, then the deflection ν can be,

$$\nu\cong F\cdot K_t(L,n). \qquad (7)$$

Apparently, when L is determined and n is a determined finite number, $K_t(L,n)$ is equal to a corresponding value. Thus, the deflection v will have linear relationship with the Force F. However, when n tends to infinity ($n\to\infty$), the convergence of the $K_t(L,n)$ is still unknown. For a specific temple, the area moments of inertia $I(x)$ have the maximum and minimum. When area moment of inertia $I(x)$ is a constant $\bar{I}$, $K_t(L,n)$ can be converted into $\bar{K}_t(L,n)$ and further calculated as follows,

$$
\begin{aligned}
\bar{K}_t(L,n) &= \left(\sum_{i=0}^{n-1}\frac{(n-i)\cdot(L-i\cdot\Delta x)}{E\cdot\bar{I}}\right)(\Delta x)^2 \\
&= \left(\sum_{i=0}^{n-1}\frac{(n-i)\cdot L-(n-i)\cdot i\cdot\Delta x}{E\cdot\bar{I}}\right)(\Delta x)^2 \\
&= \left(\sum_{i=0}^{n-1}\frac{(n-i)\cdot L}{E\cdot\bar{I}}\right)(\Delta x)^2-\left(\sum_{i=0}^{n-1}\frac{(n-i)\cdot i}{E\cdot\bar{I}}\right)(\Delta x)^3 \\
&= \frac{L}{E\cdot\bar{I}}\left(\frac{(n+1)\cdot n}{2}\right)(\Delta x)^2+\frac{1}{E\cdot\bar{I}}\left(\sum_{i=0}^{n-1}\left(i^2-i\cdot n\right)\right)(\Delta x)^3 \\
&= \frac{L}{E\cdot\bar{I}}\left(\frac{(n+1)\cdot n}{2}\right)(\Delta x)^2+\frac{1}{E\cdot\bar{I}}\left(+\sum_{i=1}^{n-1}\left(i^2\right)-\sum_{i=1}^{n-1}(i\cdot n)\right)(\Delta x)^3 \\
&= \frac{L}{E\cdot\bar{I}}\left(\frac{(n+1)\cdot n}{2}\right)(\Delta x)^2+\frac{1}{E\cdot\bar{I}}\left(\frac{(n-1)\cdot n\cdot(2n-1)}{6}-\frac{(1+n-1)\cdot(n-1)\cdot n}{2}\right)(\Delta x)^3 \\
&= \frac{L}{E\cdot\bar{I}}\left(\frac{(n+1)\cdot n}{2}\right)(\Delta x)^2+\frac{1}{E\cdot\bar{I}}\left(\frac{n-n^3}{6}\right)(\Delta x)^3. \qquad (8)
\end{aligned}
$$

Since $\Delta x=\frac{L}{n}$, then when n tends to infinity ($n\to\infty$), $\bar{K}_t(L,n)$ can be further calculated as follows,

$$\bar{K}_t(L,n)=\frac{L}{2\cdot E\cdot\bar{I}}\cdot L^2-\frac{1}{6\cdot E\cdot\bar{I}}\cdot L^3=\frac{L^3}{3\cdot E\cdot\bar{I}}. \qquad (9)$$

Thus, we can have,

$$\frac{L^3}{3\cdot E\cdot\bar{I}_{\max}}<\lim_{n\to\infty}K_t(L,n)<\frac{L^3}{3\cdot E\cdot\bar{I}_{\min}}, \qquad (10)$$

where $\bar{I}_{\max}$ and $\bar{I}_{\min}$ are the maximal and minimal $I(i\cdot\Delta x)$ for all segments, respectively. To simplify the model, we assume

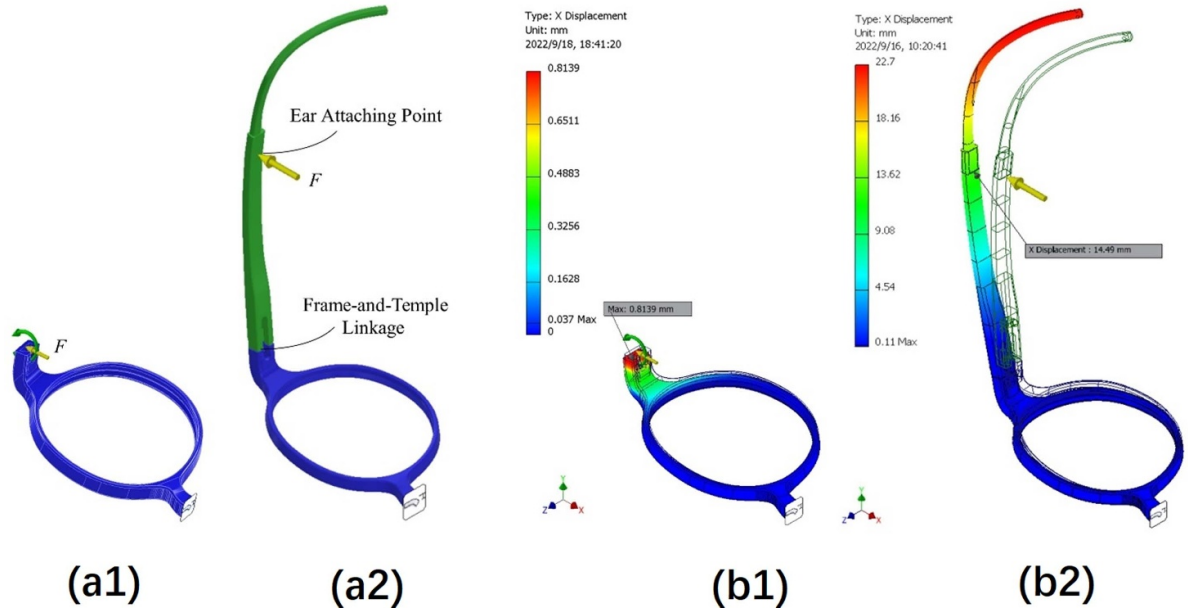

Figure 4. Examples of FEA results. (a1)/(b1) setting of loads and constrain for rim/temple. (a2)/(b2) lateral displacements for rim (clamping force $F = 0.2$ N, temple length $L = 70$ mm) / temple (clamping force $F = 0.6$ N, temple length $L = 70$ mm).

that the limitation of the series summary can converge, then we have,

$$\bar{K}_t(L,\infty) = \frac{L^3}{3 \cdot E \cdot \ddot{I}}. \tag{11}$$

Finally, we can have,

$$\nu = F \cdot \bar{K}_t(L,\infty) = F \cdot \frac{L^3}{3 \cdot E \cdot \ddot{I}}. \tag{12}$$

Since both E and $\ddot{I}$ are constants, $E \cdot \ddot{I}$ is also a constant and commonly known as flexural rigidity [9]. In the model parameters calculation, E dose not needed to be provided and $E \cdot \ddot{I}$ can be estimated as one constant from an experimental dataset (including multiple lateral displacements ν under different length L and force F).

2.2.2. Rim displacement. The rim is also considered as a cantilever beam under a force F and a pure bending $M = F \cdot L$. The structure of the rim is too complicated to be approximated by a symbol element in classical structural mechanics. Under small deformation conditions, it is reasonable to assume that the lateral deformation ω (see figure 3(a)) is proportional to the force F. Since the pure bending M is related to the distance L, let the coefficient be $K_r(L)$, then we can have,

$$\omega = F \cdot K_r(L). \tag{13}$$

Since the moment plays the leading role in deforming the frame, it was also assumed that the coefficient $K_r(L)$ is linearly related to the length L, $K_r(L) = L \cdot C_r$, where C_r is a constant (unit: 1/N). Thus, we can let,

$$\omega = F \cdot K_r(L) = F \cdot L \cdot C_r. \tag{14}$$

2.2.3. Superposed displacement. When the temple and frame displacements are superposed, the lateral displacement d (see figure 3(b)) of the ear attaching point of temple can be given as follows,

$$d = \nu + \omega = F \cdot \left(\bar{K}_t(L,\infty) + K_r(L)\right) = F \cdot \left(\frac{L^3}{3 \cdot E \cdot \ddot{I}} + C_r \cdot L\right). \tag{15}$$

In practice, when glasses are worn an individual head (see figure 1(b)), the lateral displacement d of the temple EAP is equal to the difference of the expansion distance of the EAPs on the temple under static and wearing conditions: $d = (W_{\mathrm{wt}} - W_{\mathrm{st}})/2$. The expansion distance of the EAPs under wearing condition is highly related to the head width W_{E}: $W_{\mathrm{wt}} = W_{\mathrm{E}} + 2T_{\mathrm{t}}$. Hence, the temple clamping force F for individual head can be calculated as follows,

$$F = \frac{d}{\frac{L^3}{3 \cdot E \cdot \ddot{I}} + L \cdot C_r} = \frac{W_{\mathrm{E}} + 2T_{\mathrm{t}} - W_{\mathrm{st}}}{2\left(\frac{L^3}{3 \cdot E \cdot \ddot{I}} + L \cdot C_r\right)}. \tag{16}$$

where $E \cdot \ddot{I}$ and C_r are related to the materials of the temples and can be confirmed by conducting experiments on glasses and performing experimental data analysis.

2.3. Method validation

2.3.1. Simulated validation. Since there is an assumption about rim displacement of equation (14) in section 2.2.2, we need to demonstrate it firstly. Then, we also need to validate the reliability of the developed model (i.e. equation (15)). Therefore, we utilized FEA to simulate the behavior of digital eyeglasses (see figure 4), generating a range of simulated data that captured various superposed displacements d and rim displacements ω caused by different clamping forces F and

(a) (b)

Figure 5. Physical eyeglasses for physical validation. (a) Metal eyeglasses. (b) Plastic eyeglasses.

temple lengths L. After that, we adopted regression analysis to calculate their model coefficients.

2.3.1.1. Rim displacement. To verify the above assumption about the rim displacement (i.e. equation (14)), we performed the FEA to acquire multiple lateral displacements ω under different temple length L and clamping force F in the Autodesk Inventor. The setting of load and constrain is illustrated in figure 4(a1). The middle plane (bridge) of the frame was fixed while a force and a moment were applied. The force F ranged from 0.2 N to 0.6 N at the step of 0.1 N, and L ranged from 40 mm to 100 mm at the step of 10 mm. One example of lateral displacements for rim is shown in figure 4(b1). In total, 35 sets of data (L, F, ω) were acquired and analyzed to examine the reliability of Equations 14 by using linear regression analysis [10, 11].

2.3.1.2. Superposed displacement. To demonstrate the model about the superposed displacement (i.e. equation (15)), the FEA was performed again to acquire multiple lateral displacement d under different temple length L and force F. In FEA, the force F was applied to the temple at the distance of L to the fixed end of temple, and the constrain of the half-glasses was a fixed constrain exerting on the middle plane (see figure 4(a2)). The temple length L ranged from 40 mm to 100 mm at the step of 10 mm and the force F ranged from 0.2 N to 0.6 N at the step of 0.1 N. One example of lateral displacements for rim is shown in figure 4(b2). In total, 35 sets of data (L, F, d) were obtained and analyzed to assess the reliability of equation (15) by using multiple regression analysis [10, 11].

2.3.2. Physical validation. To further demonstrate the reliability and generalization of the proposed model on physical eyeglasses, we collected the physical dataset of two eyeglasses with different materials (i.e. metal and plastic).

2.3.2.1. Metal temples. A physical dataset of metal eyeglasses (see figure 5(a)) were collected and tested. The temple length L ranged from 60 mm to 100 mm at the step of 10 mm, the one-side temple displacement d ranged from 0 mm to 9 mm as the step of 1 mm, and their corresponding clamping forces F were measured using the proposed measurement method. In total, 30 sets of data (i.e. temple length L, temple clamping force F, temple superposed displacement d) was acquired.

2.3.2.2. Plastic temples. To demonstrate the generalization of the proposed model on different eyeglasses produced by using the same materials, a physical dataset of plastic eyeglasses with different sizes were collected and tested. We firstly produced two sets of frame components (i.e. temples and rims) by using a commercial 3D printer (FORMIGA P 110 Velocis, accuracy: 0.1–0.2 mm), and we can arbitrarily assemble eyeglasses frames (without nose pads) using two (left and right) temples and one rim (some samples are provided in figure 5(b)). To better simulate the actual situations, we acquired 210 sets of rim width W_{sr}, temple length L, and temple displacement d, where the rim width W_{sr}, temple length L, and one-side temple (attachment point) displacement d ranged from 124 to 146 mm, 90 to 110 mm, and 2 to 25 mm, respectively. Then, we measured their corresponding clamping forces F using the proposed measurement method. In total, 210 sets of data (i.e. temple length L, temple clamping force F, temple superposed displacement d) was acquired.

2.4. Perceiving clamping force

Constructing the quantified correlation between the temple clamping forces and perceived comfort scores is crucial for

designing comfortable eyeglasses tailored to the target population. Theoretically, a certain displacement of the temples is necessary to produce a comfortable clamping force that prevents the eyeglasses from slipping and discomfort. Hence, we manipulated the temple displacement of the eyeglasses to generate varying clamping forces and recruited participants to evaluate their comfort levels. The study recruited 30 Chinese adolescents aged 14–17 years; the independent and dependent variables in this experiment were the clamping force and perceived comfort scores, respectively, for eyeglasses prototypes (see figure 5(b)), and the perceived comfort was evaluated using seven-point Likert scale question ($-3\sim+3$) [15]. However, compared to the previous study [15], this work aims to provide a more detailed analysis about data discretization in processing the continuous data, which is essential to construct a quantified model to predict the temple's perceived comfort score only based on objective eyeglasses and head parameters.

Given that original clamping forces are continuous, discretizing the data can enhance the representation of knowledge underlying them [16, 17]. To this end, a data discretization method was employed to convert continuous data F into discrete data $\ddot{F}$ using an interval t_f as follows: $\ddot{F} = \mathrm{Round}(F/t_f)\cdot t_f$, where $\mathrm{Round}(\cdot)$ denotes a rounding function. Several mathematical models of the perceived comfort scores of the temples are constructed and compared by using ordinary least squares (OLS) regression [10, 11] with varying force intervals. Consequently, the optimal force interval is confirmed to construct the mathematical model.

3. Results and discussions

3.1. Method validation

3.1.1. Simulated results. For the dataset (L, F, ω) of rim displacement (see blue scatters in figure 6(a)), the linear regression result (see black line in figure 6(a)) shows $C_r = 0.062$ ($R^2 = 0.998$), which demonstrates that the lateral deformation ω is proportional to the product of clamping force and temple length ($F\cdot L$):

$$\omega = 0.062\cdot F\cdot L, \left(R^2 = 0.998\right). \tag{17}$$

This indicates that we can reject the null hypothesis and conclude that it exists a linear relationship between the independent (i.e. $F\cdot L$) and dependent (i.e. ω) variables.

For the dataset (L, F, d) of superposed displacement (see color scatters in figure 6(b)), since the eyeglasses frame is made of ABS plastic, $E = 2240$ MPa; the multiple regression result (see heat map in figure 6(b)) shows $C_r = 0.2007$, $\ddot{I} = 5.044$, and $E\cdot\ddot{I} = 1.130$ GPa m^{-2} ($R^2 = 0.999$), which demonstrates the constructed model has a high reliability:

$$d = 0.0295F\cdot L^3 + 0.2007F\cdot L, \left(R^2 = 0.999\right). \tag{18}$$

In particular, P-values of two coefficients (C_r and $\ddot{I}$) are less than 0.05, which indicates significant relationships between the independent (i.e. $F\cdot L^3$ and $F\cdot L$) and dependent (i.e. d) variables.

Interestingly, we omitted the rim displacement ω and only fitted the temple displacement ν as the superposed displacement d. The new fitting equation (see figure 6(c)) was shown as follows,

$$d = 0.0551F\cdot L^3, \left(R^2 = 0.968\right). \tag{19}$$

The regression results showed $F\cdot L^3$ can significantly affect superposed displacement d (t = 32.106, p-value = 0.000) and the R^2 coefficient of determination showed that the fitting model was good.

In reality, for a new set of eyeglasses with the same materials but different sizes, the flexural rigidity ($E\cdot\ddot{I}$) of the temples can be estimated by physical experiments with regression methods. Then, this clamping force model can be used to predict the clamping force, when a pair of eyeglasses (with known temple length L, displacement d, and flexural rigidity $E\cdot\ddot{I}$) is worn a face.

3.1.2. Physical results

3.1.2.1. Metal temples. The temple clamping force model has been validated by using simulated dataset. To further demonstrate the model reliability for the physical eyeglasses, we used the dataset of metal temples (see figure 7) to calculate their fitting linear equation. The fitting surface is shown in figure 7(a) and the fitting equation is shown as follows,

$$d = 0.0293F\cdot L^3 + 0.0718F\cdot L, \left(R^2 = 0.997\right). \tag{20}$$

The R^2 coefficient of determination showed that the fitting model was good. Interestingly, we found that the equation without the term of rim displacement ω ($F\cdot L$) also has a good fitting, as follows,

$$d = 0.0405F\cdot L^3, \left(R^2 = 0.987\right). \tag{21}$$

This indicated the rim displacement ω could be ignore in the fitting model. This physical dataset of metal eyeglasses demonstrated the reliability of the constructed model.

3.1.2.2. Plastic temples. The flexural rigidity ($E\cdot\ddot{I}$) of temple is highly related to its material, shapes, and sizes. We have already demonstrate the accuracy of temple clamping force model by using metal temples. To further demonstrate the model generalization, we used the dataset of plastic temples (see figure 8) to calculate their fitting linear equation. To estimate $\ddot{I}$ and C_r, we also applied multiple regression analysis [10, 11] into the physical dataset (see scatters in figure 8(a)). The fitting surface is shown in figure 8(a) and the fitting equation is shown as follows,

$$d = 0.0316F\cdot L^3 + 0.0618F\cdot L, \left(R^2 = 0.990\right). \tag{22}$$

The regression results showed $F\cdot L^3$ can significantly affect superposed displacement d (t = 10.671, p-value = 0.000), in comparison, $F\cdot L$ had much less influences ($t = 1.988$, p-value

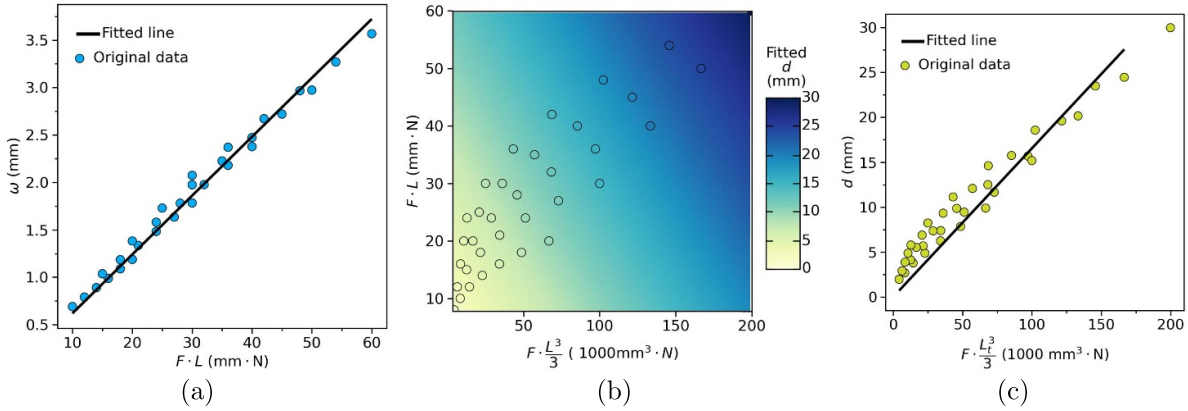

Figure 6. Regression results for simulated dataset. (a) Linear regression result for frame displacement ω. (b) Multiple regression result for superposed displacement d. (c) Linear regression result for temple displacement ν.

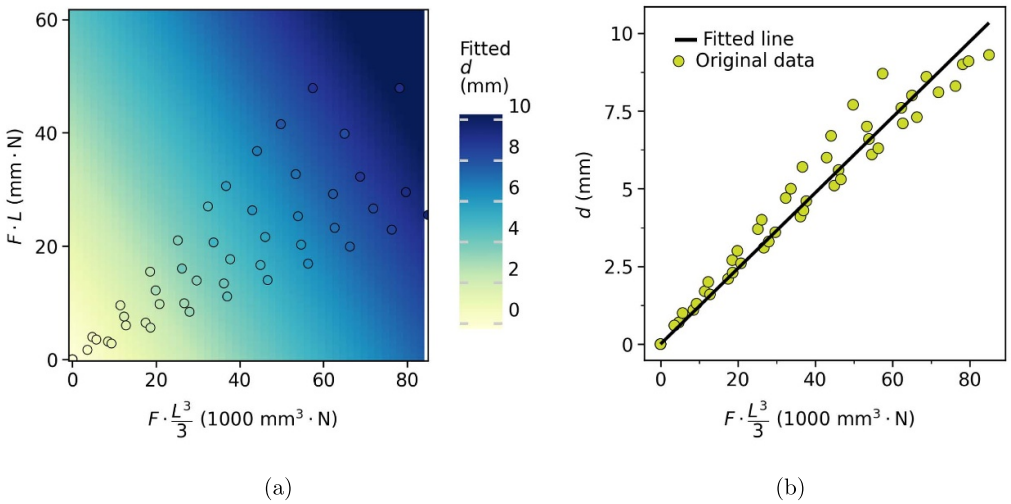

Figure 7. Regression results of physical dataset for metal temples. (a) Multiple regression result for superposed displacement d. (b) Linear regression result for temple displacement d.

$= 0.048$), which indicated that the rim displacement ω could be ignored. Hence, we omitted the rim displacement ω and only fitted the temple displacement ν as the superposed displacement d. The new fitting equation (see figure 8(b)) was shown as follows,

$$d = 0.0375F \cdot L^3, \left(R^2 = 0.989\right). \tag{23}$$

The regression results showed $F \cdot L^3$ can significantly affect superposed displacement d ($t = 139.6261$, p-value $= 0.000$) and the R^2 coefficient of determination showed that the fitting model was good, which indicated our clamping force model can be used for eyeglasses with same materials and shapes but different sizes. Hence, it is reasonable to only consider temple displacement ν and omit the rim displacement ω for superposed displacement d: $d \approx \nu = F \cdot \frac{L^3}{3 \cdot E \cdot I}$. This also demonstrated that our clamping force model had a good generalization ability for eyeglasses with different materials, e.g. plastic and metal.

3.1.2.3. Matching tests. We have added a detailed comparison of the simulation results using FEA and the physical measurements conducted on plastic eyeglasses. Specifically, the matching between the simulation and measurement results is as follows:

(1) For the simulation testing, the eyeglasses frame was modeled using ABS plastic material properties: Young's modulus (E) of 2240 MPa and the same geometric shape as the physical plastic eyeglasses. The temple length (L) was set to 100 mm, and the applied forces (F) were varied from 0.2 N to 0.6 N in 0.1 N increments. The simulation results were then fitted to a new equation: $d = 0.0498F \cdot L^3$, with an excellent coefficient of determination ($R^2 = 0.999$).

(2) To evaluate the matching between the simulation and physical measurement results, we conducted experiments using the actual plastic eyeglasses. We measured the temple displacements (d_m) under applied forces (F) ranging from 0.145 N to 0.512 N. We then used the

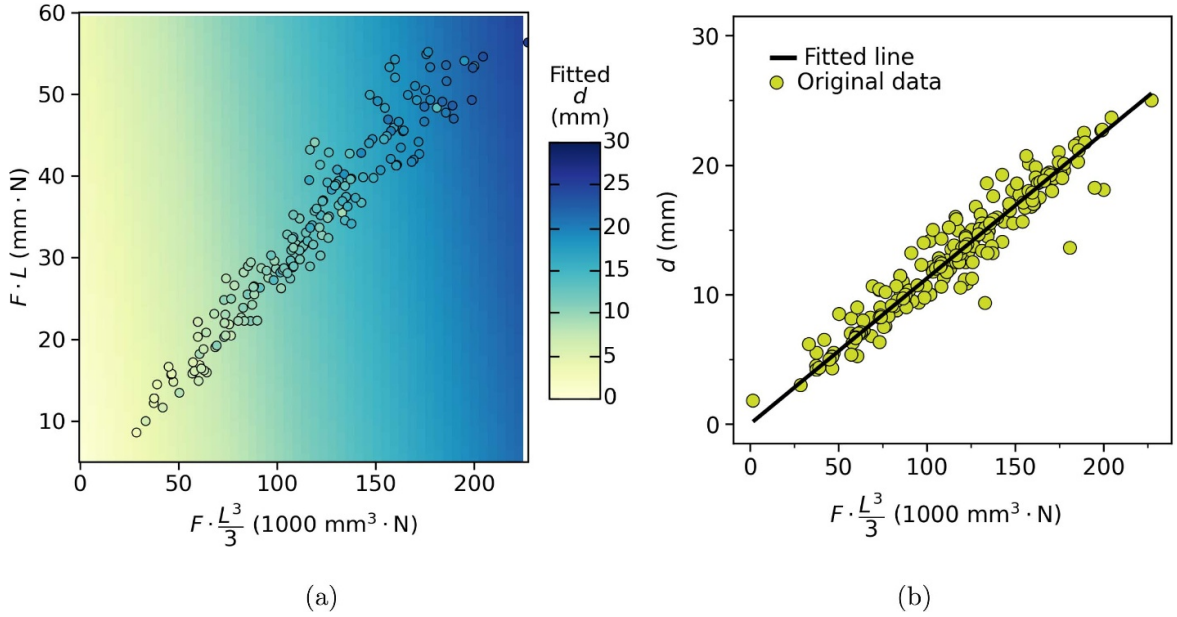

Figure 8. Regression results of physical dataset for plastic temples. (a) Multiple regression result for superposed displacement d. (b) Linear regression result for temple displacement d.

Table 1. Mathematical modeling results of perceived comfort scores for the temples using OLS regression [11, 18] with varying force intervals, including the most comfortable clamping force of prototypes under static conditions using different force intervals.

Force interval	No. Observations	Trendlines	R^2	The Largest comfort	Clamping force (N)
0.100	6	$y = -46.55x^3 + 15.68x - 1.96$	0.978	1.545	0.338
0.075	8	$y = -52.97x^3 + 19.48x - 2.89$	0.974	1.656	0.349
0.050	11	$y = -59.08x^3 + 22.10x - 3.27$	0.956	1.701	0.347
0.025	21	$y = -63.24x^3 + 22.10x - 3.27$	0.894	1.757	0.340

simulation-derived equation to compute the predicted temple displacements (d_p) for the corresponding force values.

The comparison of the measured (d_m) and predicted (d_p) temple displacements showed an average difference of 0.4335 ± 0.2678 mm. This small discrepancy, within the standard deviation, demonstrates a strong agreement between the simulation results and the physical measurements. The close matching validates the appropriateness and accuracy of the FEA modeling approach used in this study.

3.2. Users' perceptions

The mathematical modeling results of the perceived comfort scores of the temples using OLS regression [10, 11] with varying force intervals are presented in table 1 and figure 9, showing both quantitative and qualitative analyses, respectively. Different force intervals can lead to different numbers of observations, resulting in different trendlines. For all trendlines in table 1, the R^2 values were greater than 0.89, indicating a strong relationship between the two variables, and the temple clamping forces of the highest perceived comfort score ranged from 0.338–0.349 N. These findings suggest that there is no significant difference in the use of four different force intervals in the data discretization process for calculating the trendlines. Particularly, equation (16) and the trendlines in table 1 can be used to predict the perceived comfort score of the temples for a specific user based solely on the eyeglasses and head parameters. These head parameters (e.g. head width W_H) can be easily computed from 3D parameterized heads using two predefined landmarks [13, 14].

3.3. Discussions

To the best of our knowledge, ours is the first work to conduct a comprehensive study to measure and model the temple clamping force for eyeglasses. The simulated and physical datasets demonstrated the reliability of the developed model (i.e. equation (15)) for temple clamping force. In addition, equation (16) enables the computation of temple displacement using eyeglasses and head parameters, which can be used to estimate the temple clamping force for an individual with a known head width. Consequently, for a specific eyeglass product and a target population of parameterized heads [13, 14, 19, 20], it is reliable to automatically compute the clamping force for each head. If this model is combined with the quantified comfort perception model (see

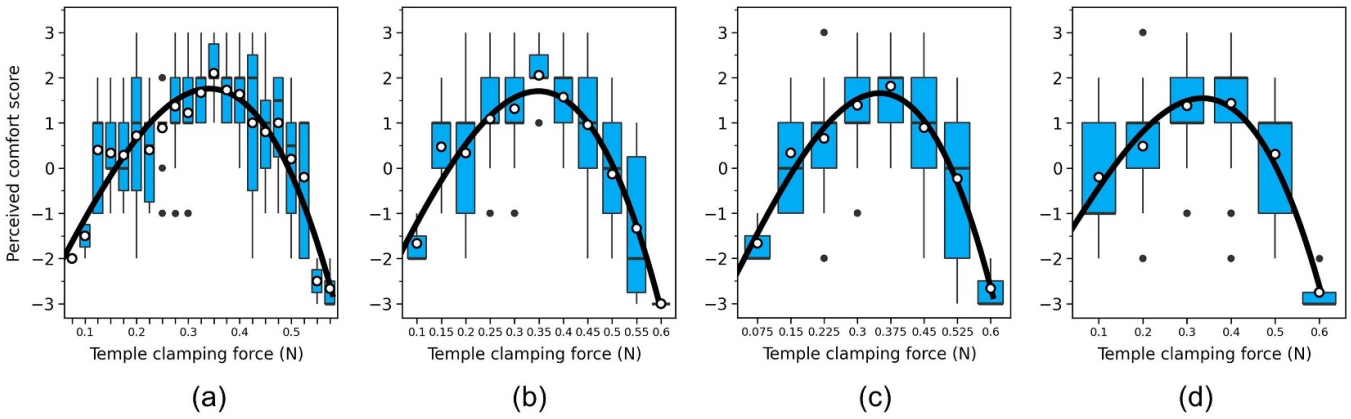

Figure 9. Fitted trendlines on the original data of temple's perceived comfort scores by using varying intervals t_f in data discretization. (a) $t_f = 0.025$. (b) $t_f = 0.050$. (c) $t_f = 0.075$. (d) $t_f = 0.100$. The blue boxplots with black dots denote the perceived comfort score distributions with outliers under varying temple clamping forces, the white scatters denotes the average perceived comfort scores, and the black lines indicate the fitted polynomial trendlines. Note that there is a polynomial relationship between the measured clamping forces and perceived comfort scores, which can be found using varying intervals in data discretization.

table 1) with the independent variable of the clamping force, it is feasible to accurately predict an individual's or group's comfort score for an eyeglasses. This would allow for a more precise assessment of comfort levels, providing valuable insights for product design and user satisfaction [21]. Therefore, we believe that our model will contribute significantly to improving the ergonomic design of a wide range of eyewear [22].

4. Conclusion

In this study, we proposed a novel method for measuring temple clamping force in eyeglasses using a digital tension meter. This method is convenient and versatile, as it can be used for temples with varying heights and materials. We also developed and validated a reliable calculation model for temple clamping force in eyeglasses design. The model was constructed using the Bernoulli-Euler beam theory and verified using simulated and physical datasets. Our experimental results demonstrate that the model can accurately predict the temple clamping force using eyeglasses and head parameters, and has good generalization ability. Finally, we conducted a temple-comfort perception experiment to demonstrate the effectiveness of our approach. We believe that this method can be extended to investigate the comfortable clamping force for various types of eyeglasses, including those designed for myopia, hyperopia, astigmatism, sunglasses, and AR glasses, and to optimize their ergonomic design.

Data availability statement

All data that support the findings of this study are included within the article (and any supplementary files).

Acknowledgments

The work described in this paper was fully supported by two grants from the Research Grants Council of the Hong Kong Special Administrative Region, China (Project No. GRF/PolyU 15606321 and 15607922).

ORCID iDs

Jie Zhang https://orcid.org/0000-0001-8219-5590
Junjian Chen https://orcid.org/0000-0002-2621-0095
Yan Luximon https://orcid.org/0000-0003-2843-847X

References

[1] Organization W H *et al* 2019 World report on vision
[2] A. R. M. Size 2021 Share report, 2022-2030 grandviewresearch. com
[3] Zhang J and Luximon Y 2017 An interview study on children's spectacle frame fit *Proc. Int. Conf. on Applied Human Factors and Ergonomics* (Springer) pp 81–88
[4] Xu J, Liu B, Wang Y and Jiang K 2022 Digital design and evaluation for additive manufacturing of personalized myopic glasses *Sci. Rep.* **12** 1–21
[5] Du Y, Liu K, Ju Y and Wang H 2022 A comfort analysis of AR glasses on physical load during long-term wearing *Ergonomics* **66** 1325–39
[6] Kouchi M and Mochimaru M 2004 Analysis of 3D face forms for proper sizing and cad of spectacle frames *Ergonomics* **47** 1499–516
[7] Mashima M, Yoshida H and Kamijo M 2011 Investigation of wearing comfort of eyeglasses with emphasis on pain around the ears *Proc. Int. Conf. on Biometrics and Kansei Engineering* pp 228–31
[8] Saadeh M Y, Carambat T D and Arrieta A M 2017 Evaluating and modeling force sensing resistors for low force applications *Smart Materials, Adaptive Structures and Intelligent Systems* vol 58264 (American Society of Mechanical Engineers) p V002T03A001
[9] Bauchau O A and Craig J I 2009 Euler-Bernoulli beam theory *Structural Analysis* (Springer) pp 173–221
[10] Montgomery D C, Peck E A and Vining G G 2021 *Introduction to Linear Regression Analysis* (Wiley)
[11] Freund R J, Wilson W J and Sa P 2006 *Regression Analysis* (Elsevier)
[12] Zhang J, Chen J, Chen L and Luximon Y 2023 A novel temple clamping force measurement method for eyeglasses design

Proc. Int. Conf. on Applied Human Factors and Ergonomics and the Affiliated Conf. pp 1–7
[13] Zhang J, Iftikhar H, Shah P and Luximon Y 2022 Age and sex factors integrated 3D statistical models of adults' heads *Int. J. Ind. Ergon.* **90** 103321
[14] Zhang J, Fu F, Shi Y and Luximon Y 2022 Modeling 3D geometric growth patterns and variations of children's heads *Appl. Ergon.* **108** 103933
[15] Zhang J, Chen J, Fu F and Luximon Y 2023 A 3D anthropometry-based quantified comfort model for children's eyeglasses design *Appl. Ergon.* **112** 104054
[16] Fu T-c 2011 A review on time series data mining *Eng. Appl. Artif. Intell.* **24** 164–81
[17] Chaudhari P, Rana D P, Mehta R G, Mistry N J and Raghuwanshi M M 2014 Discretization of temporal data: a survey (arXiv:1402.4283)
[18] Draper N R and Smith H 1998 *Applied Regression Analysis* vol 326 (Wiley)
[19] Kuo C-C, Wang M-J and Lu J-M 2020 Developing sizing systems using 3D scanning head anthropometric data *Measurement* **152** 107264
[20] Zhang J, Luximon Y and Chen L 2024 Size children's eyeglasses: an assembly-guided and comfort-oriented optimization approach based on 3D statistical ophthalmic modeling *Adv. Eng. Inform.* **59** 102266
[21] Zhang J, Luximon Y, Shah P and Li P 2023 3D statistical head modeling for face/head-related product design: a state-of-the-art review *Comput.-Aided Des.* **159** 103483:1–103483:24
[22] Balakrishnan A, Ramana K, Ashok G, Viriyasitavat W, Ahmad S and Gadekallu T R 2023 Sonar glass–artificial vision: comprehensive design aspects of a synchronization protocol for vision based sensors *Measurement* **211** 112636